1.4 MICROSTRUCTURE EVOLUTION IN TEMPERED MARTENSITIC STEELS UNDER IN-SITU He INJECTION EXPERIMENT IN HFIR JP28/29 — Takuya Yamamoto, Yuan Wu, G. Robert Odette (University of California Santa Barbara), Dan Edwards, Rick Kurtz (Pacific Northwest National Laboratory)

OBJECTIVE

The objective of this research is to characterize cavities and other microstructural evolutions in candidate 9Cr tempered martensitic steels under in situ He injection and displacement damage in HFIR.

SUMMARY

TEM studies have been carried out to observe the microstructure evolution in normalized and tempered 8-9Cr martensitic steels (TMS) Eurofer 97 and F82H under in situ helium injection (ISHI) fission reactor irradiation at nominally 500°C to ≈ 39 dpa and ≈ 2100 appm helium at 500°C. The irradiations were carried out as part of the JP-28&29 US DOE – JAEA collaboration. The cavity microstructure analyses showed cavities with an average size of ≈ 2.5 nm and number density of ≈ 2.4 x $10^{24}/m^3$, resulting in a total cavity volume fraction of ≈ 0.35%. The corresponding void volume fraction is ≈ 0.18%. The magnitude of void swelling is significantly smaller than what was previously observed at 21 dpa and 1230 appm He in JP-27 specimens. The reason for less swelling at higher dpa and He is that the intended 500°C irradiation temperature fell significantly below 500°C during the irradiation.

PROGRESS AND STATUS

Introduction

Predicting and mitigating the effects of a combination of large levels of transmutant He and displacement damage (dpa), produced by high energy neutrons on the dimensional stability and mechanical properties of structural materials is one of the key challenges in the development of fusion energy [1]. The fundamental overriding questions about He-dpa synergisms include: a) What are the basic interacting mechanisms controlling He and defect transport, fate and consequences, and how are they influenced by the starting microstructure and irradiation variables (dpa rate, He/dpa ratio, temperature and applied stress); and, b) how can the detrimental effects of He-dpa synergisms be mitigated and managed by proper microstructural design?

We have previously demonstrated that in situ He implantation (ISHI) in mixed spectrum fission reactor irradiations provides a very attractive approach to assessing the effects of He-dpa synergisms, while avoiding most of the confounding effects associated with Ni- or B-doping type experiments [1-8]. Another approach to study He-dpa synergism is to use dual ion (DI) beams to simultaneously implant He and create displacement damage with heavy ions [1,9-12]. In spite of an apparent similarity, the two techniques have many differences that include the dpa rate, the spatial distribution of damage and He and the proximity of a free surface. Nevertheless, our earlier study [10,11] indicated

- Swelling incubation dose ≈ linearly decreases with He/dpa in DI
- Larger swelling with He/dpa is consistent with limited observations in ISHI
- Swelling incubation dose in ISHI is significantly lower than in DI presumably due mainly to dpa and He implantation rates
- Post-incubation trend of swelling is nearly common when the above data are plotted on a incubation normalized dose scale

Development of a microstructure database from ISHI and DI irradiation experiments over wide range of irradiation variable conditions is an important objective of this research, and provides a basis to inform, calibrate and validate predictive models. Here we report the most recent results from the ISHI experiment carried out in the HFIR JP-28 and 29 irradiations.

Experimental Procedure

Irradiation conditions

ISHI experiments have been included in US-JAEA collaboration JP-26, 27, 28/29 and 30 target capsules and DOE-Japan MEXT collaboration TITAN program rabbit capsules both in HFIR, as well as the UCSB ATR-1 experiment. The details of ISHI method is described elsewhere, but in summary the experiment is carried out using TEM discs with a thin NiAl intermetallic coating that was electron beam deposited at UCSB. The coated discs were paired with adjacent uncoated discs as illustrated in Figure 1, so that He atoms generated in the NiAl via two-step Ni thermal neutron reactions are injected up to ≈ 9 µm deep from the surface regions of both coated and uncoated discs. Target coating thicknesses of 0.8, 1.6 and 4 µm produced nominal He/dpa ratios of 11, 22, and 55 at 39 dpa in the case of JP-28/29 capsules. Some results from the JP-26 and JP-27 capsules have been reported previously, while new JP-28/29 capsules provided specimens at higher dose and He conditions, nominally 39 dpa and 2430 appm, respectively. Table 1 summarizes those materials and irradiation conditions.

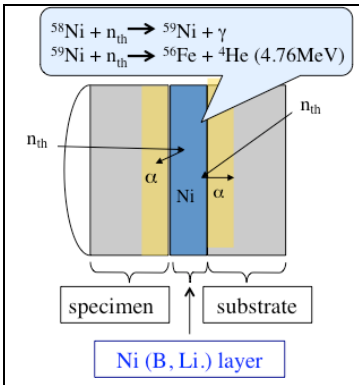

Figure 1. Schematic of in situ He injection technique

Table 1. Irradiation conditions for ISHI experiments in HFIR

Irr. ID	T(°C)	dpa	He(appm)	He/dpa(appm)	Spec ID	Material
JP26	500	9	169	18.8	R25	Eurofer 97
JP26	500	9	190	21.1	H24	F82H mod.3 (AT)
JP26	500	9	372	41.3	R26	Eurofer 97
JP26	500	9	372	41.3	R27	Eurofer 97
JP26	500	9	380	42.2	H27	F82H mod.3 (AT)
JP26	500	9	380	42.2	UN27	F82H mod.3 (CW20)
JP27	500	21	510	24.3	H57b	Eurofer 97
JP27	500	21	510	24.3	UN56	F82H mod.3 (CW20)
JP27	500	21	1230	58.6	R56	Eurofer 97
JP27	500	21	1250	59.5	UN57	F82H mod.3 (CW20)
JP28/29	500	39	858	22.0	O84	F82H_IEA
JP28/29	500	39	2145	55.0	R86	Eurofer 97

Materials

We included various materials in the experiment with emphasis on two major material groups, tempered martensitic steels (TMS) and nano-structured ferritic alloys (NFA). This report focuses on some TMS alloys with emphasis on high dose swelling trends and effects.

The TMS material group includes two heats (IEA and Mod.3) of F82H and Eurofer97 [12,13]. F82H mod.3 is one of the F82H steel variants. The base chemical composition of F82H-IEA (nominally, 7.5%Cr 2%W 0.2%V 0.1%C 0.1%Si 0.02%Ta 60ppmN), Mod. 3 is a high purity (14 ppm N and 0.001% Ti) variant of F82H with high 0.1% Ta [13]. Both heats were austenitized at 1040°C for 30 min, normalized (air-cooled), and tempered at 740°C for 1.5 h. The F82H mod.3 was also included in the 20% cold worked (CW20) condition in addition to the as tempered (AT) condition. The composition of the 6.25 mm Eurofer97 plate used in this study is: 8.93Cr, 1.08W, 0.49Mn, 0.20V, 0.12C, 0.04Si, 0.021N, < 0.01(P, Cu, Co, Ti, Nb, B), bal. Fe (wt%) [14,15]. The plate was austenitized at 980°C for 27 minutes and air-cooled prior to tempering at 760°C for 90 minutes.

PIE methods

TEM specimens were prepared by focused ion beam micromachining (FIBing) at a low final current of 5.5 pA and voltage of 2 keV. The cavities were characterized using through-focus sequence imaging. They appear as white regions surrounded by a dark ring in the under-focused condition (typically -500 to -1000

nm) and as dark regions surrounded by white rings in the over-focused condition. Cavities were identified by careful comparative image analysis of the under and over-focused micrographs. Cavities were not observed in un-implanted regions, consistent with the well-known high swelling resistance of Eurofer97 and F82H in the absence of sufficient helium. The absolute diameters of the bubbles cannot be determined precisely, especially at small sizes, without detailed corrections. The cavity diameters reported here are the nominal values for the white spot diameter in the under-focused condition. Foil thicknesses were determined by convergent beam electron diffraction.

Results

Cavity Microstructure

Figure 2a and Figure 2b show representative TEM cavity microstructure images in Eurofer 97 at (a) 21 dpa and 1230 appm He in JP-27 and (b) 39 dpa and 2145 appm He in JP28/29, both at a nominal temperature of 500°C. Fig. 3a and 3b show the corresponding size distributions of the cavities in the Eurofer 97 samples. Surprisingly, the lower dose and He condition showed more numerous large faceted cavities, which are growing voids. At higher dose, smaller ≈ 2 nm, more numerous (~3x) cavities are observed

Figure 4a and Figure 4b show TEM cavity microstructures in TMS alloys at lower He/dpa ratio ≈ 22 to 25. Figure 4a is taken from previous JP27 results on Eurofer 97 at 21 dpa and 510 appm He while Figure 4b shows the cavity microstructures in F82H IEA in JP28/29 irradiated to 39 dpa and ≈ 860 appm He, at He/dpa ≈ 22. The corresponding cavity size distributions are shown in Fig. 5a and 5b, respectively. While we do not have exactly matching specimen pairs for the He/dpa ratios, these irradiated alloys basically show similar cavity evolution behavior (shown later in Figs. 6 and 7 as general trends). We observe fewer large cavities, especially those > 10 nm, while the small cavity population seems to have grown in size and in number density at the higher dose.

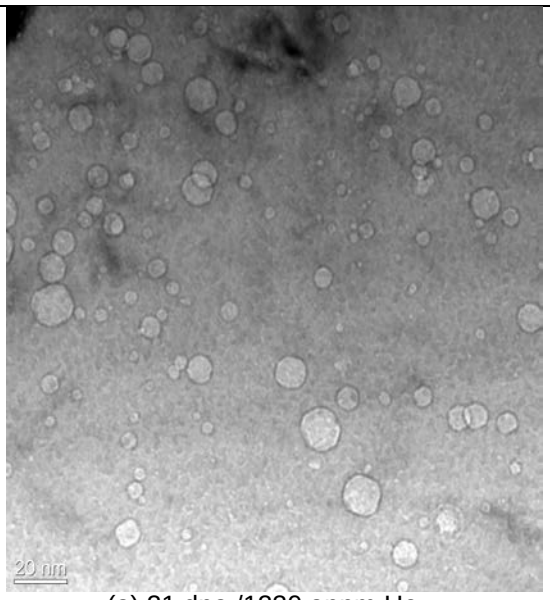

(a) 21 dpa /1230 appm He

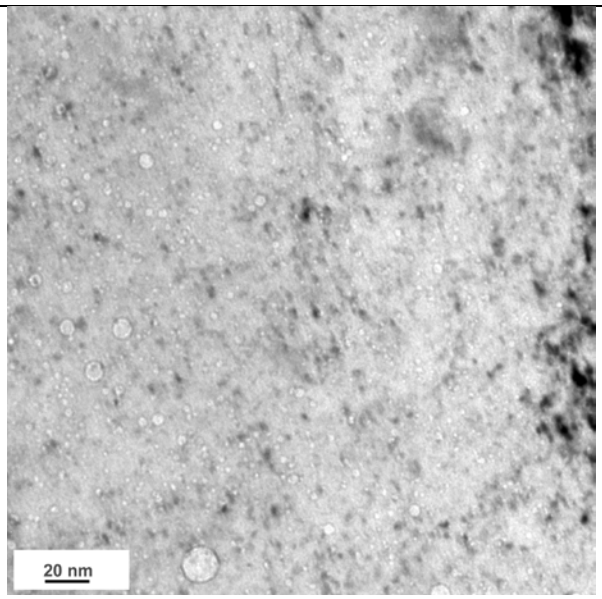

(b) 39 dpa / 2145 appm He

Figure 2. TEM cavity microstructure images in Eurofer 97 at (a) 21 dpa and 1230 appm He in JP-27 and (b) 39 dpa and 2145 appm He in JP28/29, both at a nominal temperature of 500°C

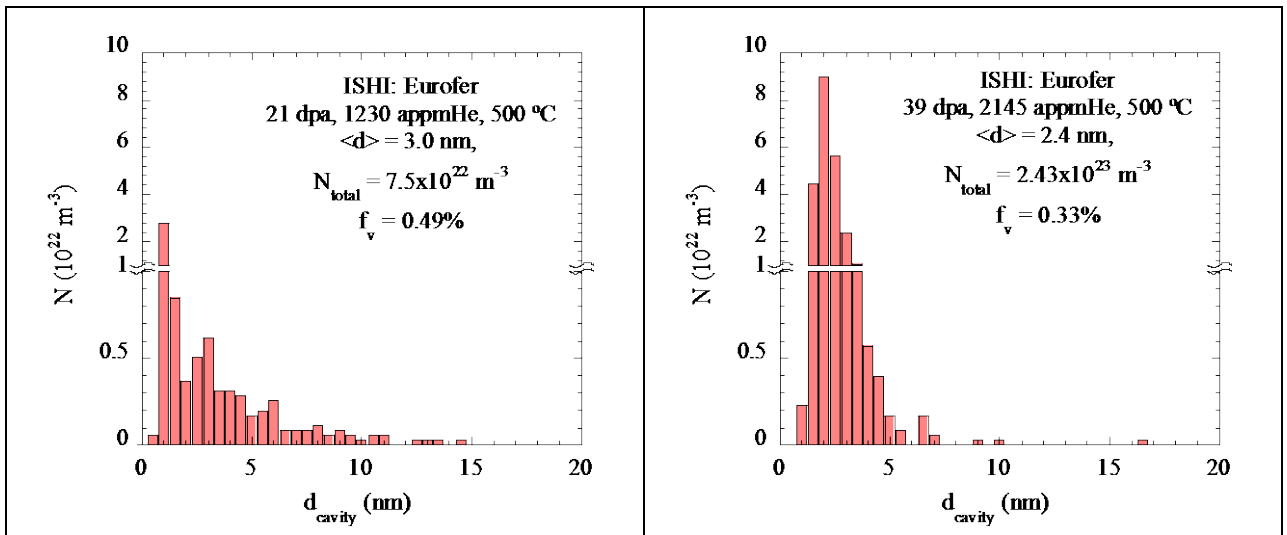

(a) 21 dpa /1230 appm He (b) 39 dpa / 2145 appm He

Figure 3. Size distribution of cavities in Eurofer 97 in situ He injected in HFIR to (a) 21 dpa and 1230 appm He in JP-27 and (b) 39 dpa and 2145 appm He in JP28/29, both at a nominal temperature of 500°C.

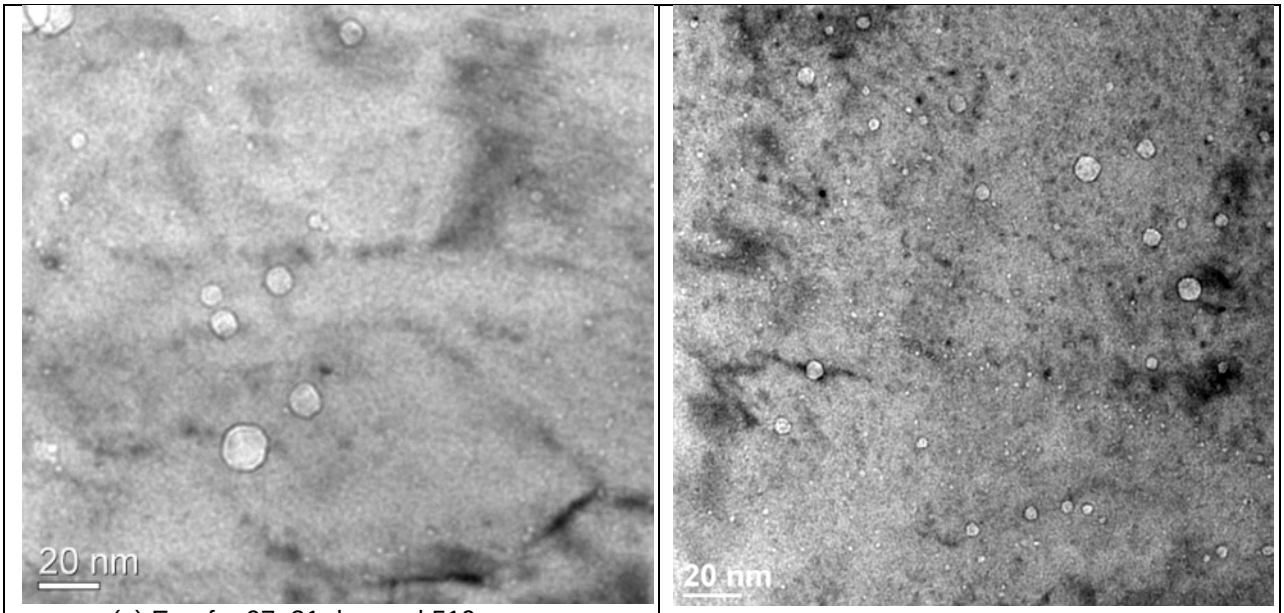

(a) Eurofer 97, 21 dpa and 510 appm (b) F82H IEA, 39 dpa and 860 appm

Figure 4. TEM cavity microstructure images in (a) Eurofer 97 at 21 dpa and 510 appm He in JP-27 and (b) F82H IEA at 39 dpa and 860 appm He in JP28/29, both at a nominal temperature of 500°C.

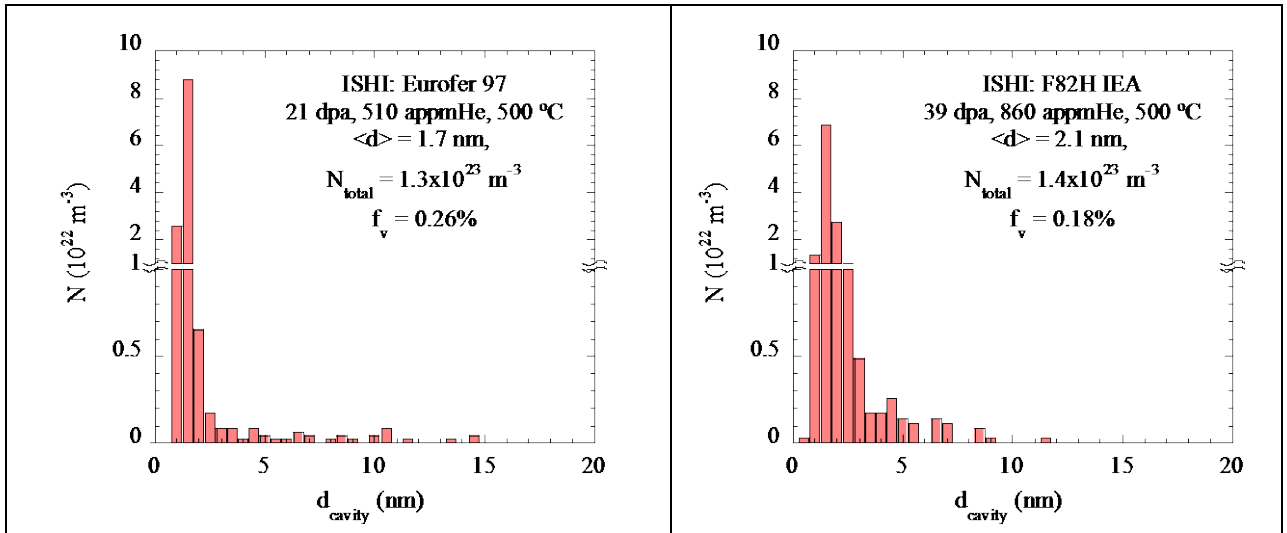

(a) Eurofer 97, 21 dpa and 510 appm (b) F82H IEA, 39 dpa and 860 appm

Figure 5. Size distribution of cavities in (a) Eurofer 97 at 21 dpa and 510 appm He in JP-27 and (b) F82H IEA at 39 dpa and 860 appm He in JP28/29, both at a nominal temperature of 500°C.

Figure 6 shows overall trends of average diameter, <d>, number density, N, and volume fraction, f, of two groups of cavities, bubbles and voids, in Eurofer 97. Here we defined voids as cavities larger than 2.25 nm, based on our earlier bi-modal distributions analyses [11]. The figures show stop of growth or even shrinkage of voids from 21 dpa to 39 dpa as well as an accelerated increase in the bubble number density.

Figure 7 shows the void evolution trends in the TMS materials. General trends are gradual (N and <d>) or rapid (f) increase from 9 to 21 dpa, while it stops or reverses from 21 to 39 dpa.

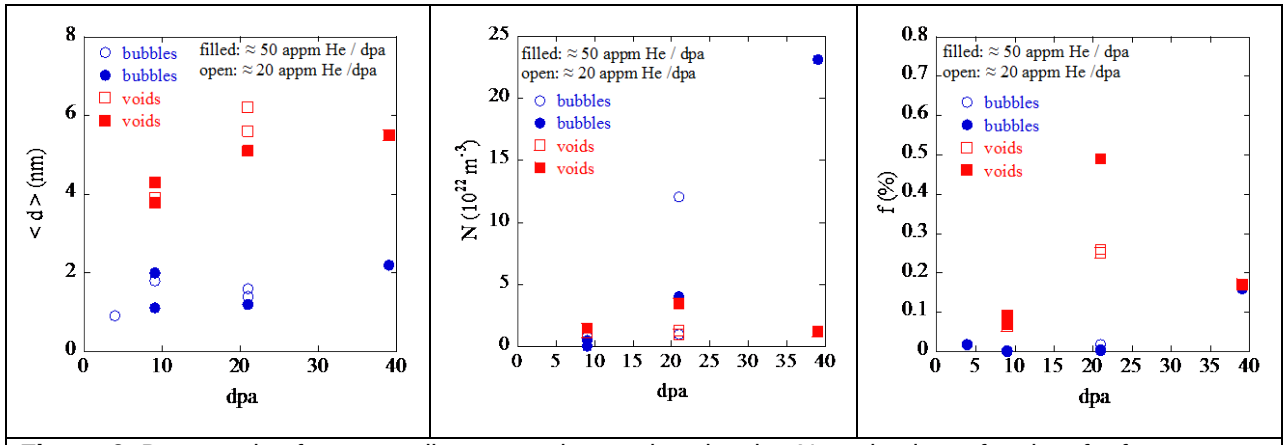

Figure 6. Dpa trends of average diameter, <d>, number density, N, and volume fraction, f, of two groups of cavities, bubbles and voids, in Eurofer 97. Voids are defined as cavities larger than 2.25 nm.

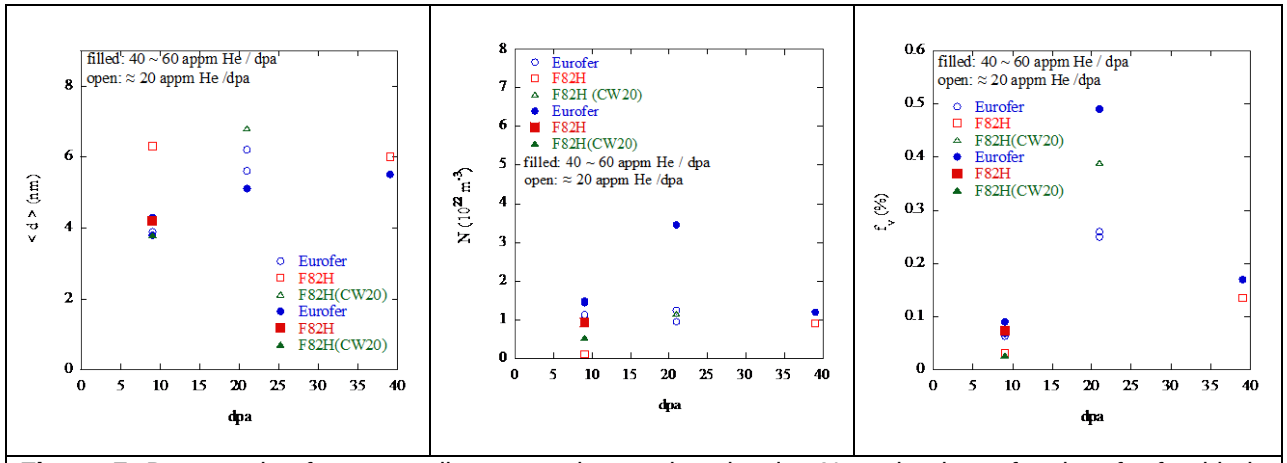

Figure 7. Dpa trends of average diameter, <d>, number density, N, and volume fraction, f, of voids in TMS alloys. Voids are defined as cavities larger than 2.25 nm.

These observations are inconsistent with the observed trend of cavity evolution between 9 and 21 dpa. Preliminary analysis of the SiC temperature monitor in another 500°C sub-capsule in the JP-28/29 capsules suggests that the irradiation temperature may have fallen off significantly, presumably due to swelling of internal parts, which reduced or closed heat transfer gaps. These observations are consistent with lower irradiation temperature conditions.

Acknowledgements

The work was supported by the U. S. Department of Energy (DOE), Office of Fusion Energy Sciences (OFES). The work performed at PNNL was supported by the U. S. ODE, OEFS, under contract DE-AC06-76RLO1830. We acknowledge the contributions of the NSF sponsored UCSB Microstructure and Microanalysis Facility, and A. L. Schemer-Kohrn, R. J. Seffens, and A. Guzman for initial specimen preparation. Authors are also grateful for the post-irradiation specimen retrieval at ORNL under the support by DOE OFES and for generous support of research materials, F82H mod.3 from Dr. K. Shiba, (JAEA, Japan).

References

[1] Y. Dai, G.R. Odette, T. Yamamoto, *The Effects of helium on irradiated structural alloys, in Comprehensive Nuclear Materials, R. Konings, T. R. Allen, R. E. Stoller, S. Yamanaka Eds. (2012) Elsevier.*

[2] T. Yamamoto, G.R. Odette, L.R. Greenwood, *Fusion Materials Semiannual Report 1/1 to 6/30/2005* DOE/ER-313/38 (2005) 95.

[3] T. Yamamoto, G.R. Odette, P. Miao, D.T. Hoelzer, J. Bentley, N. Hashimoto, H. Tanigawa, R. J. Kurtz, J. Nucl. Mater., 367-370 (2007) 399.

[4] R.J. Kurtz, G.R. Odette, T. Yamamoto, D.S. Gelles, P. Miao, B.M. Oliver, *J. Nucl. Mater.* 367-370 (2007) 417.

[5] G.R. Odette, M.J. Alinger, and B.D.Wirth, Annu. Rev. Mater. Res. 38 (2008) 471.

[6] T. Yamamoto, G.R. Odette, P. Miao, D. J. Edwards, R. J. Kurtz., J. Nucl. Mater. 386-388 (2009) 338.

[7] D.J. Edwards, R.J. Kurtz, G.R. Odette, T. Yamamoto, *Fusion Materials Semiannual Report 12/31/2009* DOE/ER-313/47 (2010) 59.

[8] G.R. Odette, P. Miao, D.J. Edwards, T. Yamamoto, R. J. Kurtz, Y. Tanigawa, J. Nucl. Mater. 417 (2011) 1001.

[9] T. Yamamoto, Y. Wu, G.R. Odette, K. Yabuuchi, S. Kondo, A. Kimura, J. Nucl. Mater. 449 (2014) 190.
[10] T. Yamamoto, Y. Wu, G.R. Odette, K. Yabuuchi, S. Kondo, A. Kimura, *Fusion Materials Semiannual Report 6/30/2015* DOE/ER-313/58 (2015) 12.
[11] G.R. Odette, T. Yamamoto, Y. Wu, S. Kondo, A. Kimura, *Fusion Materials Semiannual Report 6/30/2015* DOE/ER-313/57 (2015) 8.
[12] T. Yamamoto, Y. Wu, G.R. Odette, S. Kondo, A. Kimura, *Fusion Materials Semiannual Report 6/30/2014* DOE/ER-313/56 (2014) 194.
[13] K. Shiba, M. Enoeda, S. Jitsukawa, J. Nucl. Mater. 329-333 (2004) 243.
[14] R.J. Kurtz, A. Alamo, E. Lucon, et al., J Nuc Mat 2009; 386:411.
[15] H. E. Hofmans, NRG Report 20023/00.38153/P, 2000, Petten, The Netherlands.